Characteristics of the Marine Boundary Layer Jet over the South China Sea during the Early Summer Rainy Season of Taiwan

CHUAN-CHI TU

Department of Atmospheric Sciences, National Central University, Jhongli, Taiwan

YI-LENG CHEN

Department of Atmospheric Sciences, University of Hawai'i at Mānoa, Honolulu, Hawaii

PAY-LIAM LIN

Department of Atmospheric Sciences, and Earthquake-Disaster and Risk Evaluation and Management Center, National Central University, Jhongli, Taiwan

YU DU

School of Atmospheric Sciences, Sun Yat-Sen University, Guangzhou, China

(Manuscript received 28 June 2018, in final form 13 September 2018)

ABSTRACT

The marine boundary layer jets (MBLJs) over the northern South China Sea during the early summer rainy season over Taiwan are analyzed using 5-yr (2008–12) National Centers for Environmental Prediction Climate Forecast System Reanalysis data with a 6-h interval. The MBLJ is distinctly different from the low-level jets associated with the subsynoptic frontal systems. During this period, the MBLJ events over the northern South China Sea mainly occur during the second half of the monsoon rainy season over Taiwan (after 1 June) and have a wind speed maximum around the 925-hPa level. The MBLJs are mainly related to the subsynoptic-scale pressure gradients related to a relatively deep mei-yu trough over southeastern China and a stronger-than-normal west Pacific subtropical high. Within the MBL, there is a three-way balance among pressure gradients, Coriolis force, and surface friction, with cross-isobar ageostrophic winds pointing toward the mei-yu trough throughout the diurnal cycle. At the jet core, the vertical wind profile resembles an Ekman spiral with supergeostrophic winds $>12\,\mathrm{m\,s^{-1}}$ near the top of the MBL. The MBLJs are strongest at night and close to geostrophic flow in the late afternoon/early evening. This is because the friction velocity and ageostrophic wind decrease during daytime in response to mixing in the lowest levels. The MBLJs play an important role in horizontal moisture transport from the northern South China Sea to the Taiwan area. In the frontal zone, the moisture tongue extends vertically upward. The rainfall production is related to vertical motions in the frontal zone or localized lifting due to orographic effects.

1. Introduction

The low-level jet (LLJ) is considered one of the important factors for producing heavy orographic precipitation in many different parts of the world, such as China; Japan; Korea; the European Alps; the U.S. Sierra Nevada, Rockies, and Appalachians; and the New Zealand Alps (Lin et al. 2001; Lin 2005; Witcraft et al. 2005). Du et al. (2014) and many other previous studies classified LLJs during the early summer over East Asia into two types: 1) synoptic system–related low-level jets (SLLJs), which occur in the 900–600-hPa layer (~1–4 km), and 2) boundary layer jets (BLJs), which occur in the planetary boundary layer (PBL) below the 900-hPa level (~1 km; Chen et al. 1994; Pham et al. 2008; Du et al. 2012).

For the early summer rainy season in Taiwan, two types of LLJs were studied extensively in the literature: 1) SLLJs with maximum wind speed observed in the

Denotes content that is immediately available upon publication as open access.

Corresponding author: Dr. Yi-Leng Chen, yileng@hawaii.edu

DOI: 10.1175/MWR-D-18-0230.1

850–700-hPa layer and 2) barrier jets with a wind speed maximum ~14 m s^{-1} at approximately the 1-km level off the northwestern Taiwan coast (Chen and Yu 1988; Chen and Li 1995a,b; Li and Chen 1998; Yeh and Chen 2003).

The SLLJ is located southeast of the 850–700-hPa trough or to the southeastern flank of a lee cyclone originated in the leeside of the Tibetan Plateau or Yun-Guei Plateau over southwestern China (Chen 1977, 1978; Tao and Chen 1987; Chen et al. 1994, 1997). Chen and Yu (1988) showed when an SLLJ >12.5 m s^{-1} was present at the 700-hPa level in the warm sector of a subtropical cold front, there was a 91% likelihood that a heavy precipitation event (>100 mm day^{-1}) would occur over northern Taiwan. The development of the SLLJs in the warm sector of mei-yu fronts is largely a mass-momentum adjustment process in response to moist baroclinic forcing associated with the secondary circulation of the jet–front system (Trier et al. 1990; Chen et al. 1989, 1994, 1997; Chen and Chen 1995, 2002; Hsiao and Chen 2014).

The barrier jet off the northwest Taiwan coast is another type of low-level wind speed maximum as a result of orographic blocking. As the frontal system approaches the Taiwan area, the low-level prefrontal southwesterly flow (or SLLJ) decelerates upstream off the southwestern coast with a splitting flow over the southwestern coast as a result of orographic blocking. Along the western coast, the wind component parallel to the Central Mountain Range (CMR) increases northward down the orographically induced pressure gradients with the wind speed maximum (e.g., a barrier jet) off the northwest coast of Taiwan (Chen and Li 1995b; Li and Chen 1998; Yeh and Chen 2003). The convergence zone between the barrier jet and southwest monsoon flow and/or frontal wind shift line is the favored area for deep convection and heavy rainfall over northwestern Taiwan (Li et al. 1997; Yeh and Chen 2002; Chen et al. 2018). Also, the barrier jet transports low-level moisture from the south of Taiwan to the convergence area, which enhances convective rainfall (Kerns et al. 2010).

Recently, Chen et al. (2018) studied a heavy rainfall event during the 2012 early summer rainy season over Taiwan. For this case, in addition to localized heavy rainfall over northern Taiwan during the landfall of a mei-yu front, excessive heavy rainfall accumulation during 10–12 June prior to the passage of the mei-yu front occurred on the windward slopes on the Snow Mountains (>1000 mm) and Ali Mountains (>1500 mm) under the prefrontal SLLJ. They showed that in addition to the SLLJ, a strong low-level wind maximum with large horizontal moisture fluxes >360 g kg^{-1} m s^{-1} from the northern South China Sea to the Taiwan area was present at the 950-hPa level. In this study, this type of LLJ is referred to as a marine boundary layer jet (MBLJ). The MBLJ over the northern South China Sea during the early summer rainy season has been overlooked in the past and will be the main focus of this study.

There are different types of boundary layer jets in different parts of the world. Both the warm season LLJs over the mid-Atlantic states (Zhang et al. 2006) and the summer nocturnal low-level jets over the Great Plains (Blackadar 1957; Parish and Oolman 2010; Holton 1967; Du and Rotunno 2014) occur inland over sloping terrain. Du and Rotunno (2014) suggest that both Holton's diurnal thermal forcing over sloping terrain mechanism and Blackadar's diurnally varying boundary layer friction are important for the observed nocturnal maximum of the nocturnal low-level jets.

In addition to low-level boundary layer jets over land, there are several types of coastal boundary jets in other different parts of the world, including New York Bight jets off the coast of northern New Jersey and south of Long Island during spring and summer (Colle and Novak 2010); coastal low-level jets off the eastern China coast in July (Du et al. 2015); low-level jets off the western coast of subtropical South America (Muñoz and Garreaud 2005; Garreaud and Muñoz 2005); and easterly Caribbean LLJs in July with a secondary maximum in February (Muñoz et al. 2008; Cook and Vizy 2010). The South American LLJ events occur year-round but are most frequent during spring and summer (Garreaud and Muñoz 2005). These jets are mainly contributed by large-scale pressure gradients and enhanced by diurnal and orographic effects by the adjacent coastal terrain.

Both the Caribbean LLJs and MBLJs over the northern South China Sea occur at low latitudes (~20°N). The Caribbean LLJs are associated with the presence of the North Atlantic subtropical high (e.g., Bermuda high; Muñoz et al. 2008; Cook and Vizy 2010). During the daytime, due to land (mountains) heating to the south of the Caribbean Sea (northern South America), the southward air temperature gradient provides a baroclinic structure that intensifies the easterly winds (Muñoz et al. 2008).

The main goal of this work is to investigate the climatological characteristics of the MBLJ over the northern South China Sea, including the large-scale settings, horizontal and vertical structure, thermodynamic structure, and diurnal variations. The linkage between the SLLJs and the MBLJs on moisture transports and the possible relationship between horizontal moisture transports associated with the MBLJs and heavy rainfall over western/southwestern Taiwan will be

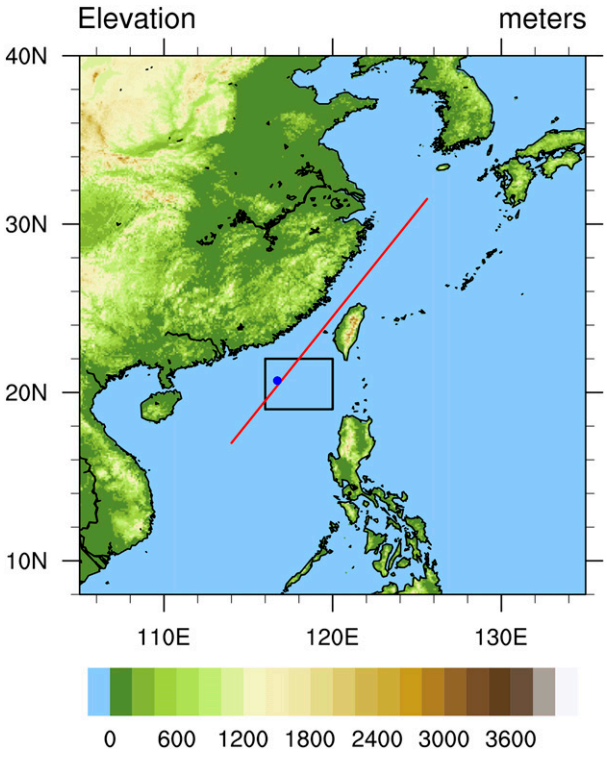

FIG. 1. Terrain height every 200 m. The black box is the region selected for the MBLJ day definition. If more than 60% of the grid points in the black box satisfy the MBLJ criteria and the event persists for more than 6 h, that entire day (0000–2400 UTC) is defined as an MBLJ day. The red line is the NE–SW cross-sectional line used in Fig. 12a. Blue dot marks Dongsha Island.

investigated. The barrier jet (e.g., orographically induced low-level strong winds) as a result of orographic blocking of MBLJ by the terrain of Taiwan will also be discussed.

2. Data and methodology

a. Criteria for identifying marine boundary layer jet days

An overall review of various criteria for identifying BLJs in the literature is given by Du et al. (2014). In this study, the National Centers for Environmental Prediction (NCEP) Climate Forecast System Reanalysis (CFSR) data from 2008 to 2012 during May/June with 0.5° × 0.5° grids at 6-h intervals and 37 pressure levels (Saha et al. 2010) are used to analyze climatological characteristics of MBLJs over the South China Sea during Taiwan's early summer rainy season. A simplified Arakawa–Schubert cumulus convection (Pan and Wu 1995; Hong and Pan 1998) with momentum mixing and orographic gravity wave drag (Kim and Arakawa 1995; Alpert et al. 1988, 1996) is used in the CFSR model. Prognostic cloud condensate (Moorthi et al. 2001) with simple cloud microphysics parameterization (Zhao and Carr 1997; Sundqvist et al. 1989) is also used. In addition to gravity wave drag, the CFSR model includes a parameterization of mountain blocking (Alpert 2004) following the subgrid-scale orographic drag parameterization (Lott and Miller 1997). The following criteria, as in Du et al. (2014), are used to identify the existence of an MBLJ over the north South China Sea: 1) maximum wind speed more than 10 m s^{-1} below the 900-hPa level and 2) below the 600-hPa level (~4 km), the wind speed must decrease by at least 3 m s^{-1} from the height of the wind maximum in the boundary layer to the wind minimum above that.

In Fig. 1, we define MBLJ days as when the black box over the northern South China Sea upstream of Taiwan is under the southwesterly monsoon flow. Similar to Du et al. (2014), if more than 60% of the grid points in the black box satisfy the MBLJ criteria and the event persists for more than 6 h, that entire day (0000–2400 UTC) is defined as an MBLJ day. The distance between the southwestern coast of Taiwan and the center of the box is about 300 km, which is considerably larger than the Rossby radius of deformation by orographic influence of Taiwan under southwesterly monsoon flow ~100 km (Li and Chen 1998). Thus, the flow close to the center of the box is representative of the upstream flow conditions impinging on southwestern Taiwan. We use data from MBLJ days to analyze the general characteristics of MBLJs during the early summer rainy season of Taiwan. Note that cases where a tropical cyclone (TC) or tropical depression (TD) is located within 8°–35°N, 105°–150°E over the western Pacific are excluded.

b. Integrated vapor transport

To delineate horizontal moisture transport associated with the MBLJs, the vertically integrated horizontal water vapor transport (hereafter, integrated vapor transport; Zhu and Newell 1998; Lavers et al. 2012) and the vertical integrals of the moisture transport components in the zonal (λ) and meridional (ϕ) directions are given as follows:

$$Q_\lambda = \frac{1}{g}\int_{P_0}^{P_1} qu\,dp, \tag{1a}$$

$$Q_\phi = \frac{1}{g}\int_{P_0}^{P_1} qv\,dp, \tag{1b}$$

where q is the specific humidity in kg kg^{-1}, u is the zonal wind in m s^{-1}, v is the meridional wind in m s^{-1}, g is the acceleration due to gravity in m s^{-2}, and p_0 is surface

TABLE 1. MBLJ days without TC or TD center located within 8°–35°N, 105°–150°E over the western Pacific (WP) in June, including 21 days (nine events).

Year	MBLJ days without TC or TD center located over WP in June
2008	15–17, 27–28
2009	2–3, 12
2010	14–15, 24–26
2011	27–28
2012	8–10, 23–25

pressure in Pa. The magnitude of the horizontal moisture transport is defined as

$$\mathrm{IVT} = \sqrt{Q_\lambda^2 + Q_\phi^2}. \tag{1c}$$

c. *Rainfall data from satellite and rain gauge observations*

Rainfall accumulation maps over Taiwan in this study are generated from rainfall stations (>300 stations have valid rainfall data), which include conventional surface weather stations and the Automatic Rainfall and Meteorological Telemetry System (ARMTS; Kerns et al. 2010). The 0.25° Tropical Rainfall Measuring Mission (TRMM; Liu et al. 2012) composite of daily rain rates during MBLJ days and June monthly rain rates from the 3B42/3B43 dataset are used to diagnose rainfall off the southwestern coast of Taiwan due to orographic blocking of MBLJ and monthly mean southwesterly monsoon flow.

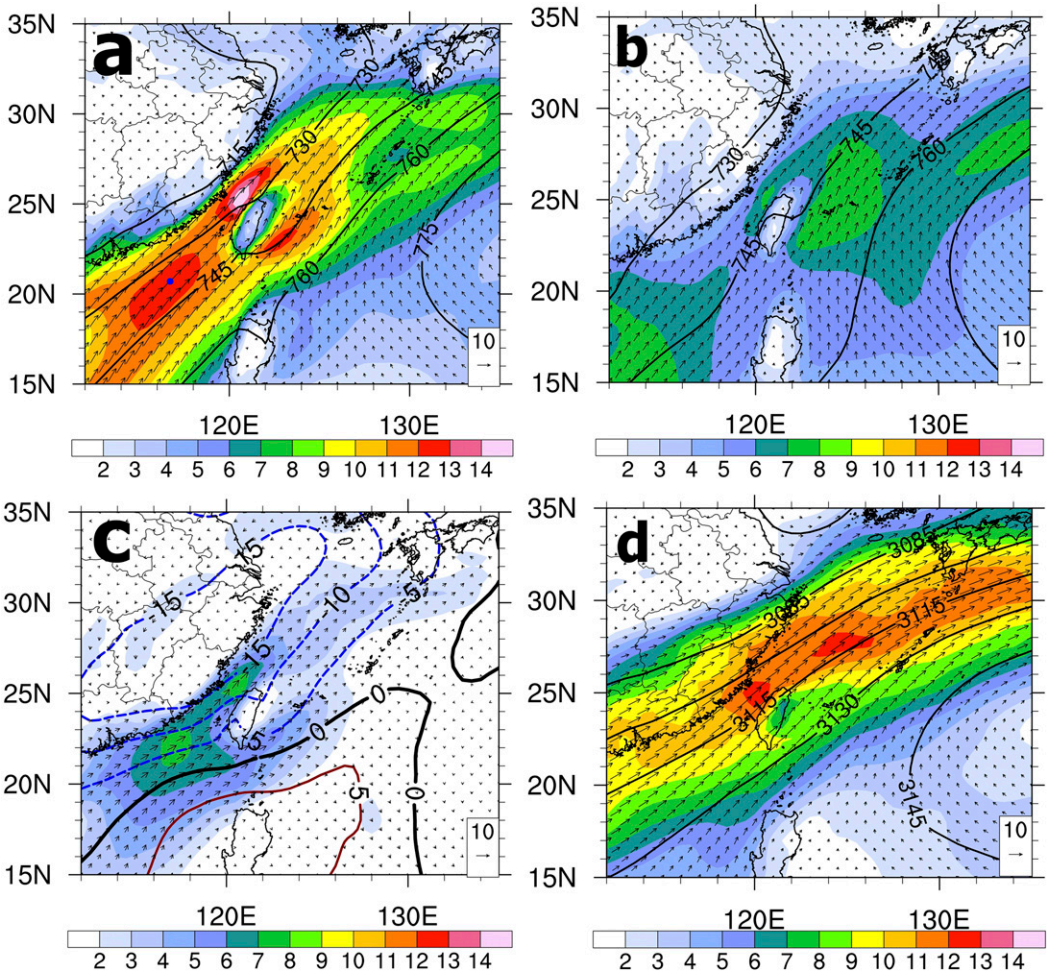

FIG. 2. The 2008–12 CFSR (a) composite of the 925-hPa winds (**V**; m s^{-1}) and geopotential height (gpm) for the MBLJ days. (b) June monthly mean 925-hPa winds (**V**; m s^{-1}) and geopotential height (gpm). (c) The 925-hPa winds (**V**; m s^{-1}) and geopotential height (gpm) differences between the MBLJ days and the June monthly mean (MBLJ days **V** − monthly mean **V**). (d) As in (a), but for the 700-hPa winds (**V**; m s^{-1}) and geopotential height (gpm). Blue solid circle in (a) marks Dongsha Island.

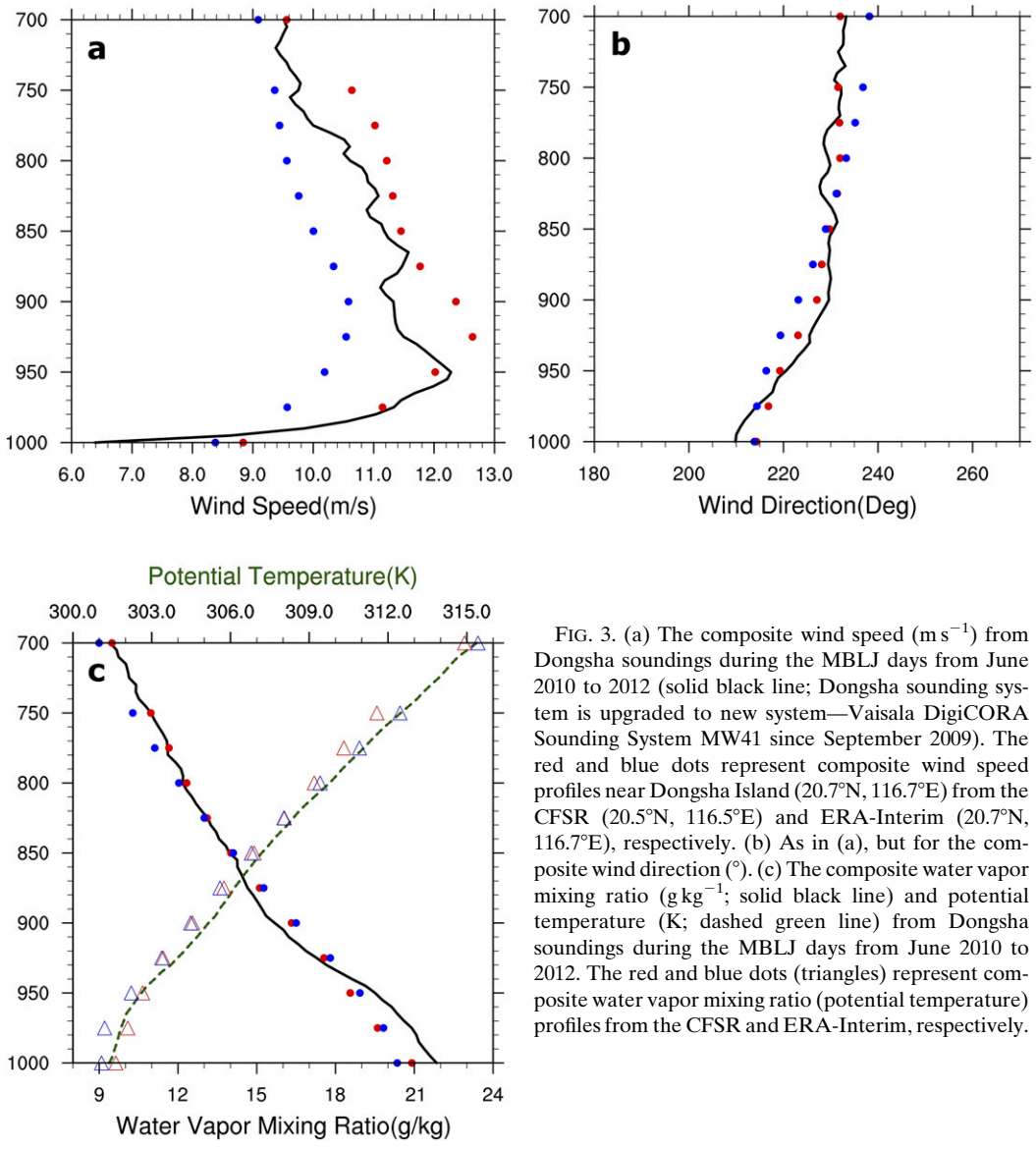

FIG. 3. (a) The composite wind speed ($m\,s^{-1}$) from Dongsha soundings during the MBLJ days from June 2010 to 2012 (solid black line; Dongsha sounding system is upgraded to new system—Vaisala DigiCORA Sounding System MW41 since September 2009). The red and blue dots represent composite wind speed profiles near Dongsha Island (20.7°N, 116.7°E) from the CFSR (20.5°N, 116.5°E) and ERA-Interim (20.7°N, 116.7°E), respectively. (b) As in (a), but for the composite wind direction (°). (c) The composite water vapor mixing ratio ($g\,kg^{-1}$; solid black line) and potential temperature (K; dashed green line) from Dongsha soundings during the MBLJ days from June 2010 to 2012. The red and blue dots (triangles) represent composite water vapor mixing ratio (potential temperature) profiles from the CFSR and ERA-Interim, respectively.

3. Results

a. Climatological features of marine boundary layer jets

The 2008–12 CFSR composite of 925-hPa winds and geopotential height for MBLJ days (Table 1) shows that the intense southwesterly monsoon flow ($>10\,m\,s^{-1}$) covers almost the entire northern South China Sea with the jet core just upstream of southwestern Taiwan (Fig. 2a). The mei-yu trough over southern China is to the northwest of the jet core, and the west Pacific subtropical high (WPSH) is to the southeast. The June monthly mean 925-hPa winds upstream of Taiwan ($\sim 6\,m\,s^{-1}$) do not reach the low-level jet criteria (Fig. 2b). From the differences in geopotential height and winds between MBLJ days and monthly mean fields for June, it is evident that during MBLJ days, the mei-yu trough over southern China is deeper, and WPSH is stronger and extends farther westward (Fig. 2c) with larger horizontal pressure gradients over the northern South China Sea (Fig. 2a), as compared to the June monthly mean (Fig. 2b).

The sounding data at Dongsha over the northern South China Sea (Fig. 1) are used to verify the CFSR and ERA-Interim (Dee et al. 2011) for the MBLJ. We used 2010–12 June data from the Central Weather Bureau (CWB) new Dongsha sounding system—Vaisala DigiCORA Sounding System MW41, operating since

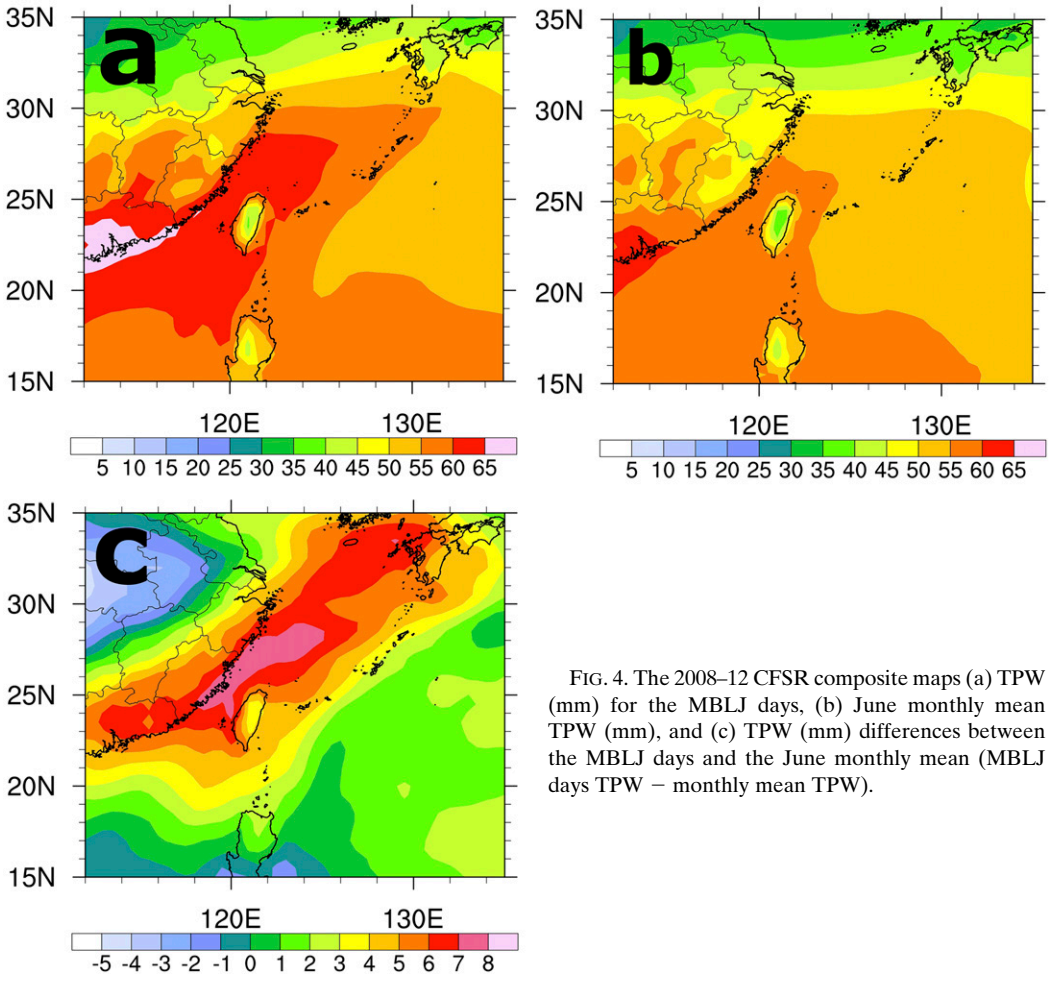

FIG. 4. The 2008–12 CFSR composite maps (a) TPW (mm) for the MBLJ days, (b) June monthly mean TPW (mm), and (c) TPW (mm) differences between the MBLJ days and the June monthly mean (MBLJ days TPW − monthly mean TPW).

September 2009. The composite ERA-Interim wind speed profile during the MBLJ days slightly underestimates the wind speed of the MBLJ, compared to the soundings (Fig. 3a). The composite CFSR wind profile agrees reasonably well with the Dongsha soundings, except the jet level is slightly lower in observations (~950 hPa), as compared with the CFSR (~925 hPa) (Fig. 3a). For the wind direction at Dongsha during the MBLJ days, both the CFSR and ERA-Interim data agree well with soundings, except wind direction is slightly more uniform in both CFSR and ERA-Interim data, as compared with observations (Fig. 3b). Both CFSR and ERA-Interim data underestimate the moisture in the lowest layer with slightly smaller vertical gradients of the potential temperature (Fig. 3c). From wind and thermodynamic profiles in low levels (Fig. 3), it appears that vertical turbulence mixing in the mixed layer of the CFSR is slightly overestimated. We also found that during MBLJ days, the Pearson correlation coefficient between the sounding observations and CFSR (ERA-Interim) is 0.76 (0.70) for the wind speed and 0.80 (0.80) for the wind direction. Note that the correlation for Dongsha soundings and CFSR is slightly higher than the ERA-Interim data.

From the horizontal distribution of total precipitable water (TPW), it is apparent that when an MBLJ occurs, a moisture tongue extends from the northern South China Sea to Taiwan area (Fig. 4a), and the moisture over the northern South China Sea is higher, compared to the June monthly mean (Fig. 4b). From the differences in TPW between MBLJ days and monthly mean, in addition to more moisture over the northern South China Sea, there is another northeast (NE)–southwest (SW)-oriented moisture axis extending from northeast of Taiwan to southeastern China (Fig. 4c). The NE–SW-oriented moisture axis (Fig. 4c) corresponds well with the low-level upward motion associated with the mei-yu trough axis (see Fig. A1 in appendix A).

With a grid size of 50 km, the orographic effects are underestimated. Vertical motion due to orographic blocking

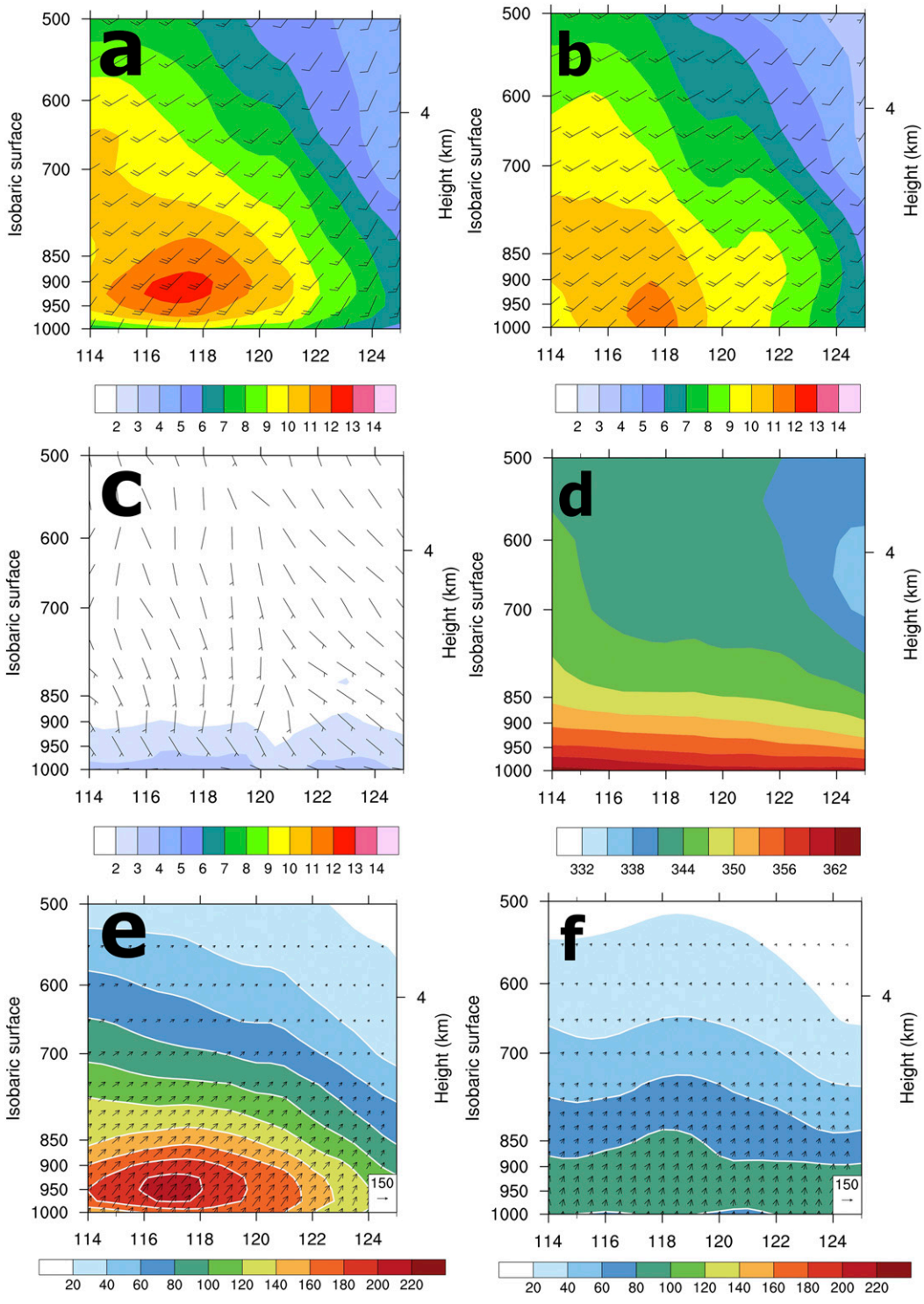

FIG. 5. (a) The 2008–12 CFSR composite of the vertical cross section along 21°N for the MBLJ days (a) winds (**V**; m s^{-1}) with wind barb (full barb represents 5 m s^{-1}), (b) geostrophic winds (Vg; m s^{-1}) with wind barb (full barb represents 5 m s^{-1}), (c) ageostrophic winds (Va; m s^{-1}) with wind barb (full barb represents 5 m s^{-1}), (d) equivalent potential temperature (K), and (e) horizontal moisture flux vector (q**V**) (g kg^{-1} m s^{-1}). (f) As in (e), but for June monthly mean.

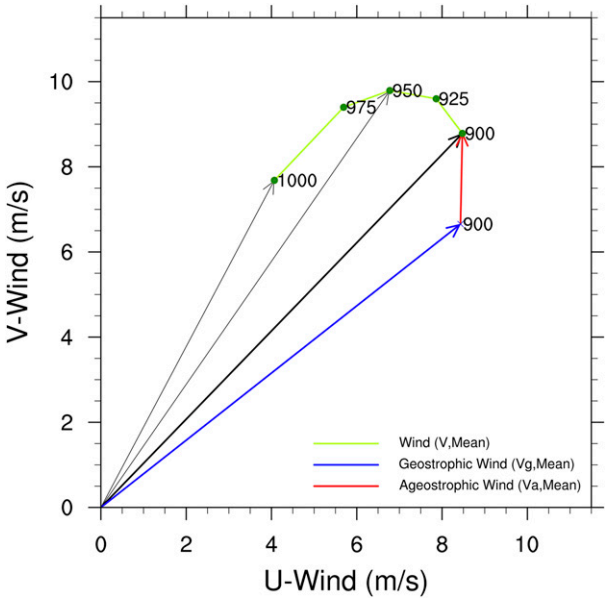

FIG. 6. The hodograph at the jet core of the MBLJs (20.5°N, 116.5°E); the green curve is the hodograph from the 1000- to 900-hPa level. The thick black arrow shows the 900-hPa winds (**V**; m s^{-1}). The thick blue arrow shows the 900-hPa geopotential winds (Vg; m s^{-1}). The thick red arrow shows the 900-hPa ageostrophic wind (Va; m s^{-1}).

is evident off the southwestern Taiwan coast when an MBLJ is present, as compared to climatology (Fig. A1). Furthermore, the barrier jet off the northwestern Taiwan coast is also stronger on MBLJ days than the June monthly mean, as the MBLJ flow impinges on the island terrain (Figs. 2a–c). In the future, high-resolution models with a grid spacing <3 km will be used to diagnose the effects of orographic blocking on the MBLJ over the Taiwan area.

b. *Structure and characteristics of MBLJs*

From the vertical cross section along 21°N across the MBLJ jet core, it is apparent that the maximum wind speed of the MBLJ occurs within the 900–950-hPa layer (Fig. 5a). At the 925-hPa level, geostrophic winds are the main contributors (~90%) to the MBLJ, with large horizontal pressure gradients (Figs. 5a–c). The ageostrophic winds over the northern South China Sea have a cross-contour component pointing toward lower pressure (Fig. 5c). Our result is similar to the schematic force balance on a fluid parcel at different heights in a barotropic PBL, with a supergeostrophic wind near the top of the MBL (Figs. 5 and 6; Arya 1985). Within the MBL, the vertical wind profile at the jet core resembles an Ekman spiral (Holton 2004; Mellor 1996; Fig. 6). The ageostrophic winds are most significant with relatively weak winds near the surface (Figs. 5a,c). The supergeostrophic wind over the MBLJ region extends from the 950-hPa level up to the 850-hPa level, and the winds gradually approach the geostrophic winds above (Figs. 5a,b). The geostrophic wind speed maximum is at the lowest levels and decreases with respect to height (Fig. 5b). The warm, moist, high equivalent potential temperature air is mainly confined within the lowest 1 km. The relatively dry and stable air is present above the MBLJ core, near the top of the MBL (<1 km; Figs. 5a,d and 3).

The low-level jet at the 850- and 700-hPa levels associated with a mei-yu front (Chen and Yu 1988) is a subsynoptic feature as part of the secondary circulation

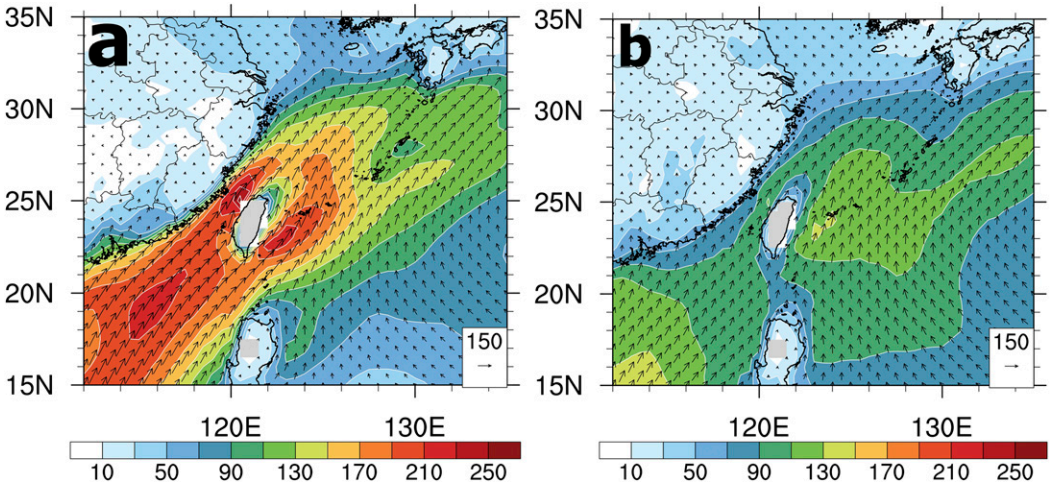

FIG. 7. The composite maps for the MBLJ days during 2008–12 using CFSR data. (a) IVT (kg m^{-1} s^{-1}) in the boundary layer (below 900 hPa). (b) As in (a), but for June monthly mean. The vectors in (a),(b) show the direction of IVT.

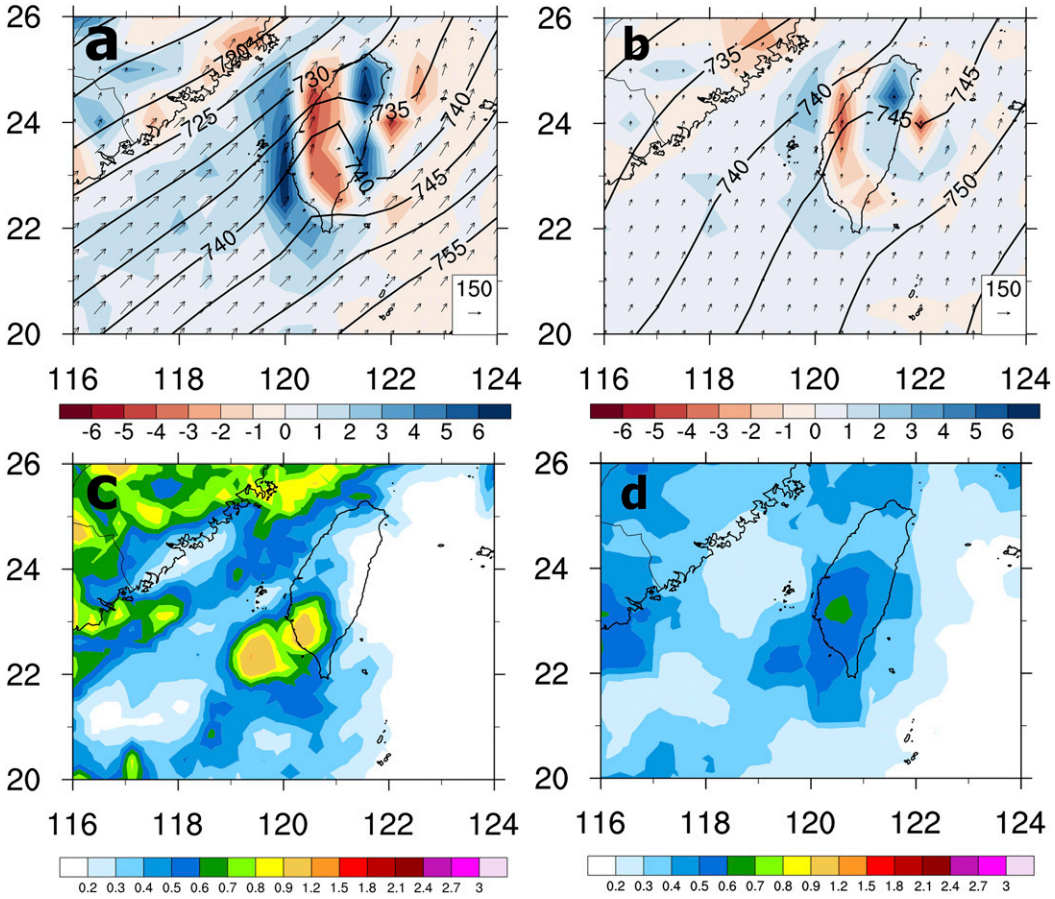

FIG. 8. (a) The 2008–12 CFSR composite of the 925-hPa moisture flux convergence (10^{-4} g kg^{-1} s^{-1}; shaded), geopotential height (gpm; contoured), and moisture flux (g kg^{-1} m s^{-1}; vectors) for the MBLJ days. (b) As in (a), but for the June monthly mean. (c) The 2008–12 0.25° TRMM composite of rain rates (mm h^{-1}; shaded) from the 3B42 dataset for the MBLJ days. (d) As in (c), but for the June monthly mean.

associated with the jet–front system (Chen et al. 1994, 1997). However, the MBLJ is a large-scale feature associated with the southwesterly monsoon flow. The main reason for the presence of the MBLJ is related to large-scale pressure gradients, as the MBLJ is dominated by geostrophic winds and modified by the boundary layer process. Not every mei-yu trough over southern China has an MBLJ over the northern South China Sea. The MBLJ is more frequent in the second half of Taiwan's mei-yu season in June, after the WPSH is well established, and less frequent during the onset phase in late May (Table 1).

For both the 15–17 June 2008 and the 8–11 June 2012 cases (Table 1), the deepening of the mei-yu trough over southern China is related to the development of a mesoscale mei-yu frontal cyclone in the leeside of the Yun-Guei Plateau (southeastern arm of the Tibetan Plateau) that migrated and extended eastward along the mei-yu trough (Fig. 4 of Tu et al. 2017; Fig. 4 of Chen et al. 2018). The deepening of the mei-yu frontal cyclone is related to a moist baroclinic process related to the north–south thermal contrast and latent heat release (Chen et al. 1997; Chen and Chen 2002). An SLLJ will be present if the mei-yu trough deepens (Chen and Chen 1995). An MBLJ over the northern South China Sea will be present only if the deepening of the mei-yu trough is concurrent with the strengthening of the WPSH (Fig. 2c). The presence of the MBLJ over the northern China Sea does not require the passage of a mei-yu front over Taiwan (Tu et al. 2014, 2017; Xu et al. 2012).

The horizontal moisture fluxes along the east (E)–west (W) cross section (~21°N) during the MBLJ days are compared with the June monthly mean. During the MBLJ days, significant horizontal moisture fluxes over the MBLJ region occur within the PBL with the maximum axis (>200 g kg^{-1} m s^{-1}) at the 950-hPa level (Fig. 5e). For the June monthly mean, the horizontal moisture fluxes associated with the southwesterly

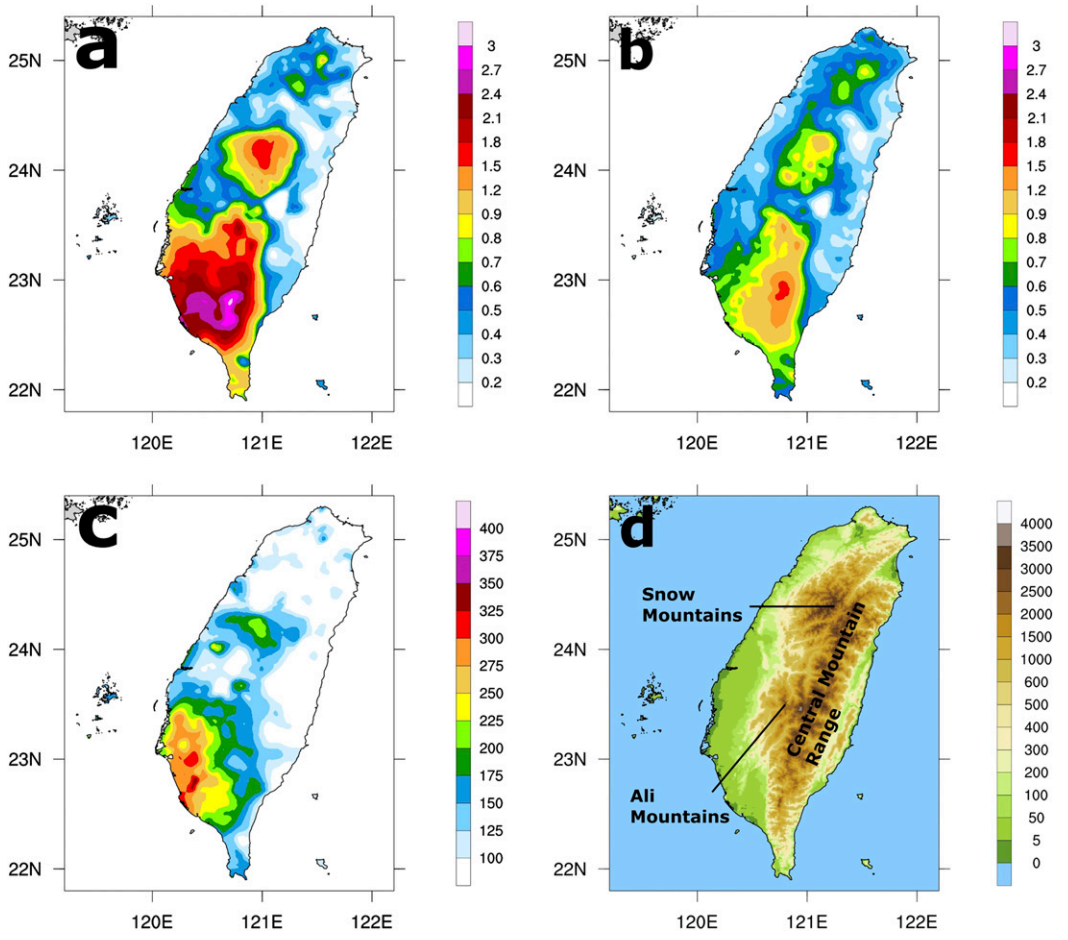

FIG. 9. The 2008–12 (a) composite of rain rates (mm h^{-1}; shaded) for the MBLJ days and (b) June monthly mean from rain gauge observations. (c) The ratio of composite rain rates for the MBLJ days to June monthly mean rain rates (%) [(a)/(b)]. (d) Terrain height (m) over Taiwan.

monsoon flow are much weaker ($<100\,g\,kg^{-1}\,m\,s^{-1}$) than the MBLJ days (Fig. 5f). In the boundary layer, the large integrated vapor transport (IVT; $>210\,kg\,m^{-1}\,s^{-1}$) covering almost the entire northern South China Sea corresponds with the MBLJ (Figs. 2a and 7a), with the IVT maximum upstream of Taiwan. The monthly mean IVT upstream of Taiwan for June is rather weak ($<110\,kg\,m^{-1}\,s^{-1}$) due to weaker PBL winds (Figs. 2b and 7b) and lower moisture content (Figs. 4a,b).

The orographic blocking of moist MBLJs results in low-level moisture convergence over southwestern Taiwan and offshore (Fig. 8a). Significant horizontal moisture fluxes associated with the MBLJs over the northern South China Sea provide abundant moisture that supports the occurrences of heavy rainfall events over southwestern Taiwan (Fig. 8c). During the MBLJ days, relatively large low-level moisture transport (Figs. 7a and 8a) and moisture convergence within the boundary layer (Fig. 8a) are present. For the June monthly mean, the horizontal moisture fluxes within the planetary layer (Fig. 8b) and the rainfall amounts over southwestern Taiwan and offshore are much less, as compared to the MBLJ days (Figs. 8c,d).

Rain gauge observations are used to provide rainfall information over Taiwan. For the June monthly mean, the moist southwesterly monsoon flow interacts with the Taiwan terrain (e.g., orographic lifting and blocking), which produces a rainfall maximum along the southwestern slopes of the CMR and a considerable amount of rain over southwestern Taiwan, the southwestern slope flank of the Snow Mountains, and the Ali Mountains (Figs. 9b,d). During the MBLJ days, with a much more intense southwesterly moisture flux (Figs. 5e,f and 7) impinging on and lifted by the Ali Mountains and Snow Mountains, the southwestern slopes of these mountains receive 150%–250% of rainfall, as compared to the monthly mean value (Fig. 9). Also during the MBLJ days, the southwestern coastal plain receives

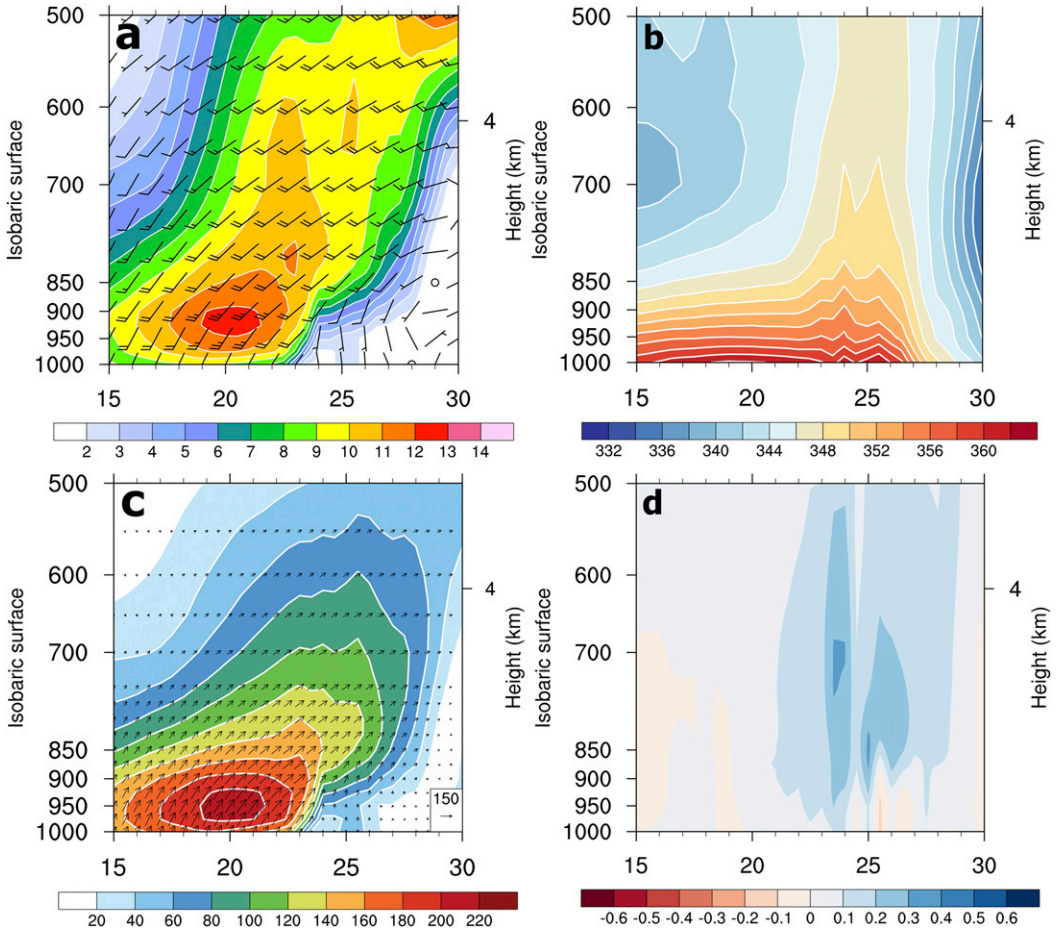

FIG. 10. The 2008–12 CFSR composite of the vertical cross section along 116.5°E for the MBLJ days. (a) Horizontal winds (**V**; m s^{-1}) with wind barb (full barb represents 5 m s^{-1}), (b) equivalent potential temperature (K), (c) horizontal moisture flux vector (q**V**; g kg^{-1} m s^{-1}), and (d) vertical moisture flux (qw; g kg^{-1} m s^{-1}).

more than 250% of rainfall, as compared to the monthly mean value, as a result of orographic blocking of MBLJ (Fig. 9). For the coastal heavy rainfall case during the Terrain-Influenced Monsoon Rainfall Experiment (TiMREX) intensive observing period (IOP) 8 case on 16 June 2008, orographic blocking of the warm, moist southwesterly low-level jet by terrain, enhanced by the presence of a cold pool, is an important factor for the production of coastal heavy rainfall under favorable large-scale settings (Xu et al. 2012; Tu et al. 2014, 2017). Note that the TiMREX IOP 8 case meets the criteria for an MBLJ event in this study (15–17 June 2008; Table 1).

c. *The relationship between MBLJ and SLLJ*

Previous studies have suggested the importance of the SLLJ in bringing moisture from the south to the mei-yu frontal zone (e.g., Chen and Yu 1988). In this section, the linkage between the MBLJ and the SLLJ in moisture transports will be examined. In addition, the relationship between the MBLJ and the barrier jet off the northwest coast of Taiwan and orographically induced strong low-level winds over the eastern side of Taiwan (Fig. 2a) will be discussed.

From the north (N)–south (S) cross section along 116.5°E across both the strong low-level winds over the northern South China Sea (Fig. 2a) and the moisture tongue along the southern China coast (Fig. 4a), the MBLJ over the northern South China Sea exhibits a maximum wind speed around the 925-hPa level (Fig. 10a), whereas the SLLJ (~23°N) associated with the mei-yu frontal system over southeastern China has a wind speed maximum within the 700–850-hPa layer (Fig. 10a). From horizontal maps, the SLLJ axis lies from the area northeast of Taiwan southwestward to the southeastern China coast (Fig. 2d). The MBLJ core is over the northern South China Sea to the south of the 700-hPa SLLJ axis (Fig. 2). From the N–S vertical cross section along 116.5°E, the SLLJ (~23°N) is associated

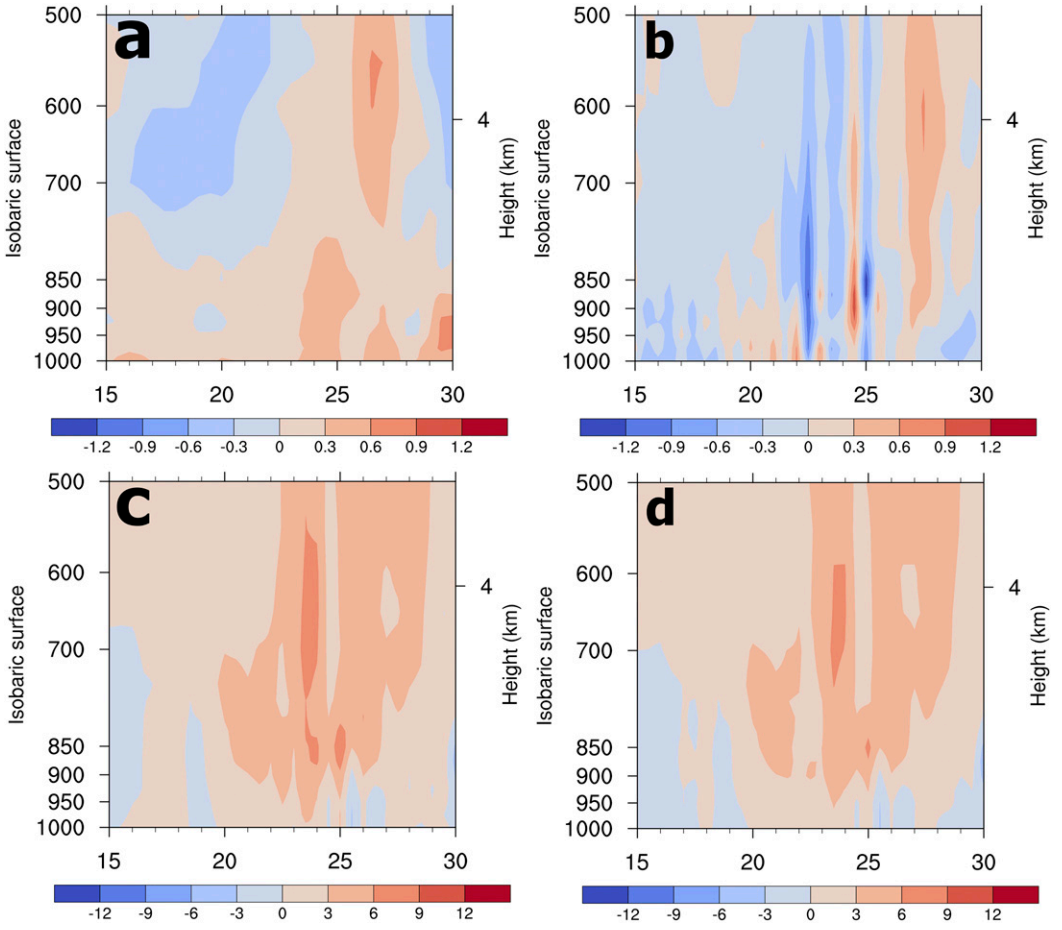

FIG. 11. The 2008–12 CFSR composite of the vertical cross section along 116.5°E for the MBLJ days. (a) The tendency term $(\partial\overline{q}/\partial t)$ $(10^{-5}\,\mathrm{g\,kg^{-1}\,s^{-1}})$, (b) horizontal moisture advection term $(-\overline{\mathbf{V}}\cdot\nabla\overline{q})$ $(10^{-5}\,\mathrm{g\,kg^{-1}\,s^{-1}})$, (c) vertical moisture advection term $[-\omega(\partial\overline{q}/\partial p)]$ $(10^{-5}\,\mathrm{g\,kg^{-1}\,s^{-1}})$, and (d) subgrid-scale term $[(\overline{c}-\overline{e})+(\partial\overline{q'\omega'}/\partial p)]$ $(10^{-5}\,\mathrm{g\,kg^{-1}\,s^{-1}})$.

with the sloping frontal surface where the low-level wind shift occurs. The MBLJ is around 20°N, south of the surface frontal zone and the SLLJ (Fig. 10a).

In the MBLJ region over the northern South China Sea, high moisture content is confined within the PBL (<1 km; Fig. 10b). Within the MBLJ, the horizontal moisture fluxes dominate (Fig. 10c). Moreover, due to a higher moisture content and stronger wind speed for the MBLJ, the horizontal moisture fluxes are more significant for the MBLJ than the SLLJ (Fig. 10c). In the sloping front zone, the warm, moist tongue extends vertically upward (Fig. 10b) as the low-level warm, moist air in the frontal zone is lifted vertically upward by the secondary circulation associated with the jet–front system (Figs. 10b,d). Over the postfrontal region, the northeasterly flow at low levels is relatively cold and dry with low equivalent potential temperature (Figs. 10a,b). The horizontal moisture transport in the postfrontal flow is not significant (Fig. 10c). The horizontal moisture fluxes associated with the MBLJs are significantly higher than the vertical moisture fluxes in the frontal zone owing to rather weak vertical motions (~1–10 cm s^{-1}) associated with secondary circulation of the jet–front system (Fig. 10). It is apparent that the vertical moisture transport in the frontal zone mainly takes place in the protected cores of convective cells (Riehl and Malkus 1958).

The moisture budget equation is given in Eq. (2) (Yanai et al. 1973):

$$\frac{\partial\overline{q}}{\partial t}=-\overline{\mathbf{V}}\cdot\nabla\overline{q}-\overline{\omega}\frac{\partial\overline{q}}{\partial p}-[(\overline{c}-\overline{e})+(\partial\overline{q'\omega'}/\partial p)], \quad (2)$$

where q is specific humidity, t is time, $\mathbf{V}$ is the horizontal wind vector, ∇ is the horizontal gradient operator, p is pressure, ω is vertical pressure velocity, c is the rate of condensation per unit mass of air, and e is the rate of

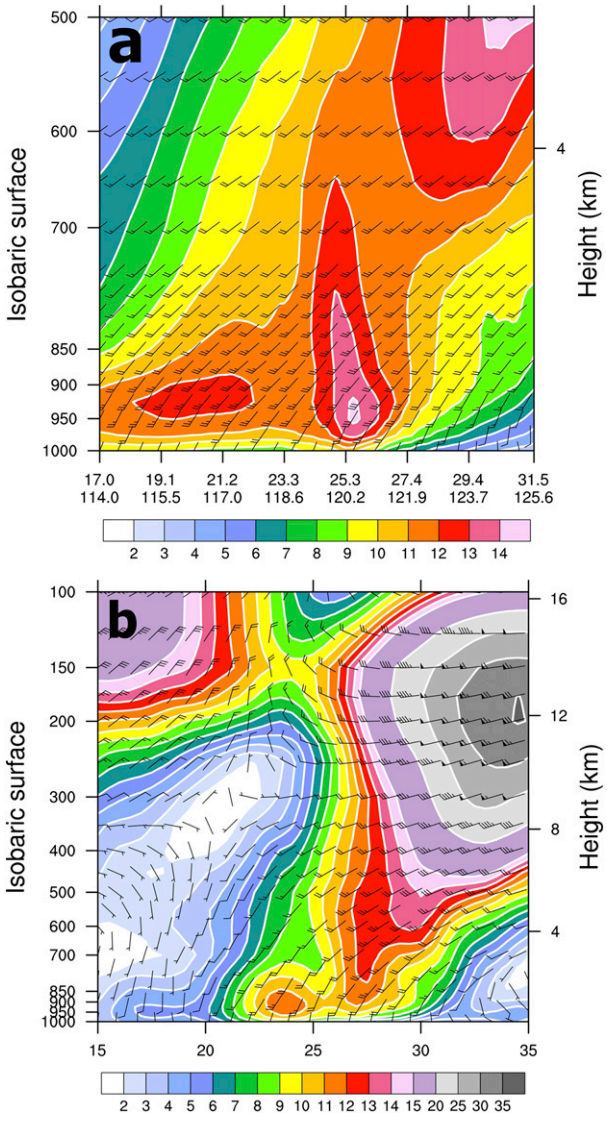

FIG. 12. (a) Vertical cross section of horizontal winds ($m\,s^{-1}$; full barb represents $5\,m\,s^{-1}$) along (a) NE–SW red line in Fig. 1 and (b) 124°E.

evaporation. The overbar refers to a horizontal average over the grid box, and the prime denotes deviations from this average. This equation is used to diagnose the moisture balance associated with the MBLJ and in the frontal zone. For climatological features (e.g., MBLJs), or long-term mean, the tendency term is rather small (Fig. 11a). From the vertical cross section along 116.5°E, it is apparent that the horizontal advection term is an order of magnitude smaller than the vertical moisture advection term (Figs. 11b,c). The tendency term has the same order of magnitude as the horizontal advection term (Figs. 11a,b). The vertical advection term and the subgrid-scale term $[(\overline{c}-\overline{e})+(\partial\overline{q'\omega'}/\partial p)]$ are the two dominant terms in the moisture budget (Figs. 11c,d). In other words, the rainfall production is mainly caused by vertical motions in the frontal zone or orographic lifting.

Li and Chen (1998) and Chen and Li (1995b) showed the presence of a barrier jet at about 1-km level along the northwestern coast of Taiwan when the southwesterly SLLJ impinges on the southwestern slopes of the CMR as the surface front approaches. In addition, strong orographically induced winds are also observed off the southeastern coast of Taiwan. In this study, the analysis of CFSR data shows the presence of a barrier jet off the northwestern coast of Taiwan as a result of orographic blocking of the MBLJ (Fig. 2a), although the jet core ($\sim 14\,m\,s^{-1}$) is slightly lower (~ 0.5 km; Fig. 12a). The barrier jet due to orographic blocking of the MBLJ is apparent at the 950-hPa level and merges with the SLLJ above (Figs. 2 and 12a). The MBLJ has a wind maximum around the 950–900-hPa layer over the northern South China Sea, with decreasing wind speed aloft (Fig. 12a).

On the eastern side of Taiwan, a localized low-level (~ 950 hPa) wind speed maximum ($11–12\,m\,s^{-1}$) is also present around 24°N (Fig. 12b), associated with orographic blocking of the MBLJ. The orographically induced strong winds are limited to the boundary layer (Figs. 2 and 12b) and separated from the SLLJ because the jet axis of SLLJ is farther north. From the N–S cross section along 124°E, the low-level (~ 950 hPa) orographically induced local wind speed maximum ($\sim 11–12\,m\,s^{-1}$), the SLLJ with wind speed maximum at the 850–700 hPa level ($>12\,m\,s^{-1}$), and the upper-level jet core are located around 24°, 27°, and 34°N, respectively (Fig. 12b). For a heavy rainfall case during 11–12 June 2012, with high-resolution (<3 km) simulation, the wind maximum of the low-level (~ 950 hPa) barrier jet associated with the MBLJ over the northern South China Sea exceeds $20\,m\,s^{-1}$ (Chen et al. 2018).

d. Diurnal variations

In this section, the 925-hPa winds from the CFSR data at 0800, 1400, 2000, and 0200 LST are compared and separated into geostrophic wind and ageostrophic wind components. Furthermore, the vertical profiles of horizontal winds at the jet core at these four different analysis times during the diurnal cycle are studied to assess the impact of diurnal friction variation on the MBLJ.

Figure 13 shows that the MBLJ is weakest in the late afternoon/early evening at 2000 LST and strongest at 0200 LST. The deepening of the mei-yu trough is mainly related to the subsynoptic process rather than the land surface heating of continental China in the afternoon hours. In addition to the subsynoptic process, the

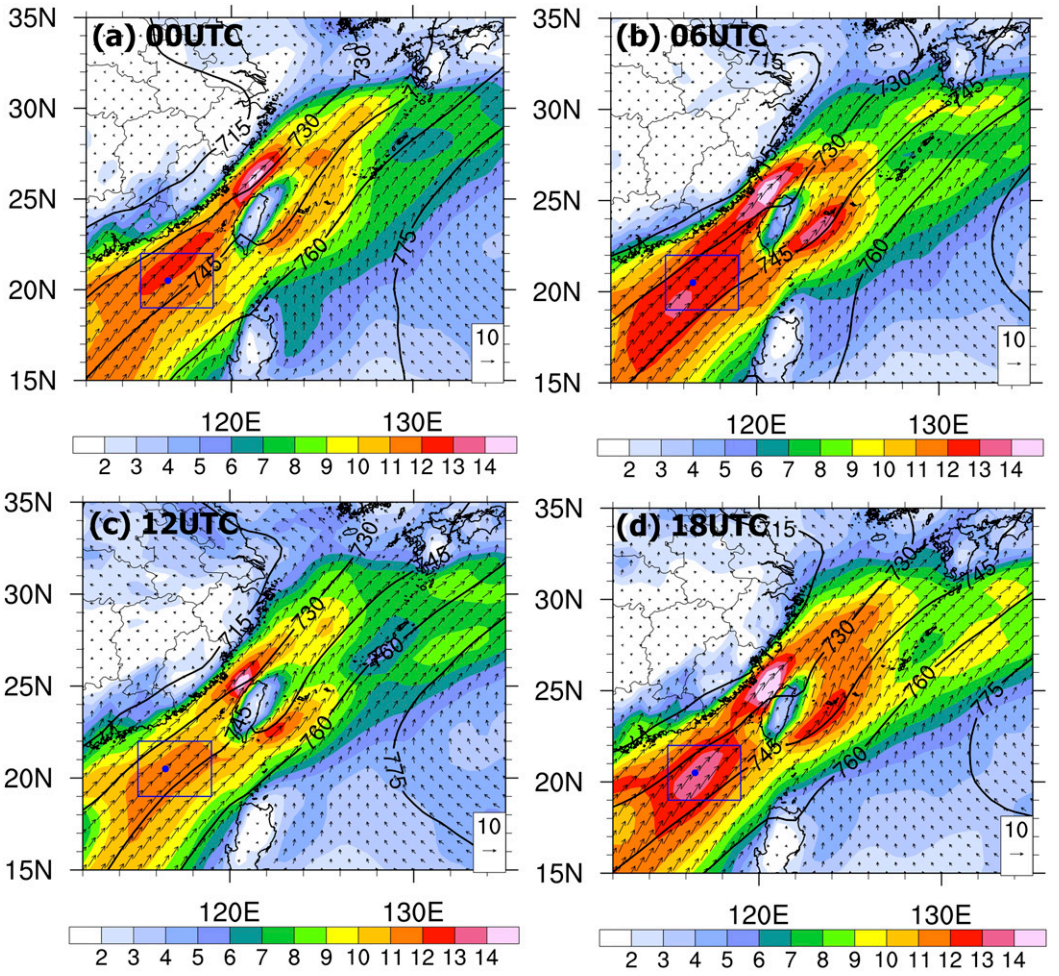

FIG. 13. Diurnal cycle of 925-hPa winds ($m\,s^{-1}$) for the MBLJ days: (a) 0000 UTC (0800 LST), (b) 0600 UTC (1400 LST), (c) 1200 UTC (2000 LST), and (d) 1800 UTC (0200 LST). Blue dot and box are used for Figs. 6, 15, and B1, respectively.

large-scale pressure gradients are modified by the semidiurnal tide over the northern western Pacific and the heating and cooling over land (Huang et al. 2010).

Diurnal variations of SST are rather small. Over the boxed area in Fig. 13, the SST daily maximum minus minimum is ~0.13°C. The wind profile in the MBL resembles an Ekman spiral throughout the diurnal cycle with the smallest cross-contour ageostrophic winds in the late afternoon/early evening (see Fig. B1 in appendix B). Around early evening (2000 LST), the airflow near the top of the boundary layer is close to the geostrophic flow and is supergeostrophic during the rest of the day (Figs. 15 and B1) due to diurnal variations in the surface friction velocity. During the nighttime, the cross-contour ageostrophic winds increase as the surface friction velocity increases (Figs. 14 and 15). The ageostrophic winds that point to lower pressure are most significant during nighttime (0200 LST; Figs. 15 and B1). It appears that the slight late afternoon minimum in the MBLJ is related to a reduction in surface friction velocity due to mixing at the lowest levels. Results from high spatial and temporal model data are required to diagnose the dynamics and diurnal variations of MBLJ further.

4. Summary and conclusions

The climatological characteristics of the MBLJ over the northern South China Sea during the early summer rainy season of Taiwan are first reported in this study. The MBLJ is distinctly different from the SLLJs, which occur in the 850–600-hPa layer (~1.5–4 km) associated with the secondary circulation of the mei-yu frontal systems during the early summer rainy season. The MBLJs over the northern South China Sea mainly occur

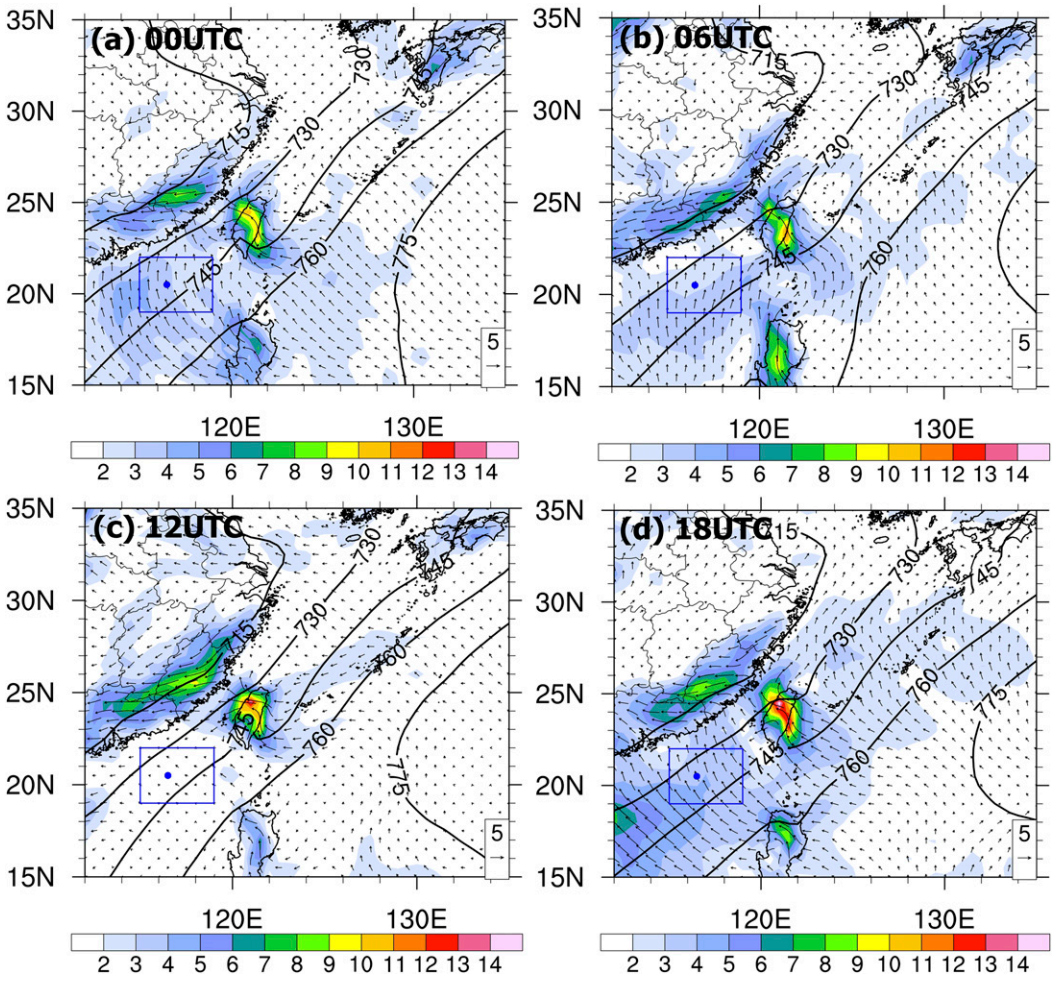

FIG. 14. As in Fig. 13, but for the 925-hPa ageostrophic winds ($m\,s^{-1}$).

during the second half of Taiwan's monsoon rainy season in June (Table 1) and have a wind speed maximum around the 925-hPa level. Because it occurs over the open ocean, it is also distinctly different from the orographically induced low-level barrier jet along the northwesterly coast of Taiwan. The barrier jet occurs when an SLLJ or an MBLJ interacts with the CMR.

The MBLJ days were determined based on vertical wind profiles from the CFSR within 8°–35°N, 105°–150°E. We found that during the MBLJ days, the mei-yu trough over southeastern China is deeper, and the WPSH is stronger and extends more westward than the climatological mean. The MBLJs are mainly caused by the subsynoptic-scale horizontal pressure gradients with cross-contour ageostrophic winds pointing toward the mei-yu trough over southern China. At the jet core, the vertical profiles of horizontal winds resemble an Ekman spiral with a wind speed maximum near the top of the MBL, where the flow is supergeostrophic throughout almost the entire diurnal cycle with a 6-h interval. At 2000 LST, the flow at the jet core is close to the geostrophic flow, with the weakest ageostrophic winds during the diurnal cycle corresponding to a decrease in surface friction velocity due to mixing at the lowest levels during the daytime.

During the MBLJ days, the MBLJs play an important role in horizontal moisture transport from the northern South China Sea to the Taiwan area. In the frontal convergence zone, the moisture tongue extends vertically upward due to the presence of vertical motion associated with the jet–front system. The rainfall production in the frontal zone or over southwestern Taiwan is mainly related to vertical motions. It is apparent that orographic blocking and lifting of the moist MBLJs by the terrain and local winds provide the localized lifting needed for the development of heavy rainfall over southwestern Taiwan and offshore. In addition, a barrier jet ($\sim$14 $m\,s^{-1}$) at the 950-hPa level is observed off the northwestern coast of Taiwan when an MBLJ is present. On the eastern side, strong ($\sim$11–12 $m\,s^{-1}$) localized

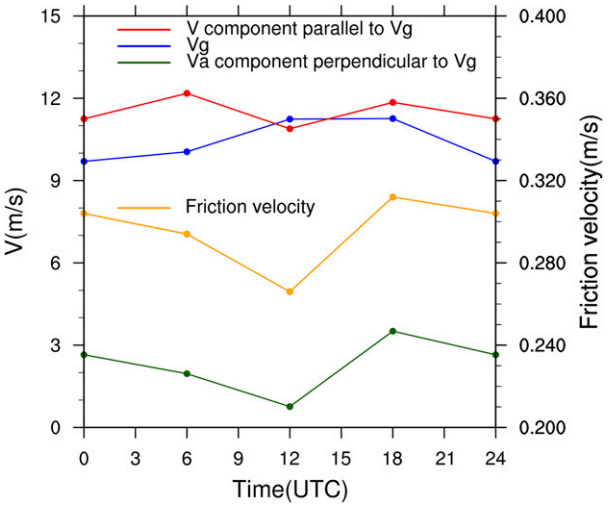

FIG. 15. Diurnal variations of the CFSR wind component parallel to the geostrophic flow ($m\,s^{-1}$; red line), the speed of the geostrophic flow ($m\,s^{-1}$; blue line), the ageostrophic wind component perpendicular to the geostrophic flow ($m\,s^{-1}$; green line), and friction velocity ($m\,s^{-1}$) for the MBLJ days over the boxed area (19°–22°N, 115°–119°E; blue box in Fig. 13).

orographically induced low-level (~950 hPa) winds are also present off the eastern coast.

In the future, we will perform the momentum balance of the MBLJ over the northern South China Sea and its diurnal variations based on hourly high-resolution (<9 km) model output. We found that the 0.5° CFSR data with a 6-h interval are inadequate to fully resolve the diurnal and terrain effects (e.g., orographic blocking of MBLJ). A high-resolution (~3 km) model nested within the 9-km regional domain will be used to study the interactions among MBLJs, diurnal and orographic effects, and rainfall distribution over the Taiwan area, as compared to observations. An MBLJ within the southwesterly monsoon flow could also be present between the WPSH and a tropical storm (or a mesoscale low-pressure center) over the northern South China Sea/southern China. Observations from an existing dense network over Taiwan and special facilities deployed during the South China Sea Two Island Monsoon Experiment (SCSTIMX) and the Prediction of Rainfall Extremes Campaign in the Pacific (PRECIP)/Taiwan-Area Atmospheric and Hydrological Observation and Prediction Experiment (TAHOPE) in 25 May–10 August 2020 will be analyzed to study the MBLJ and its possible impacts on the occurrences of heavy rainfall over the Taiwan area under favorable large-scale settings.

Acknowledgments. The Dongsha sounding data are available from the Central Weather Bureau, Taipei, Taiwan. The rain gauge data were downloaded from the Data Bank for Atmospheric and Hydrologic Research (https://dbahr.narlabs.org.tw/). This work is jointly funded by the Taiwan National Science Council (NSC) under Grant NSC-100-2119-M-008-041-MY5; by the Ministry of Science and Technology (MOST) under Grants MOST 104-2923-M-008-003-MY5, MOST 106-2811-M-008-073, and MOST 107-2111-M-008-038; and by the Featured Areas Research Center Program within the framework of the Higher Education Sprout Project by the Ministry of Education (MOE) to the National Central University, the National Science Foundation under Grant AGS-1142558 to the University of Hawai'i at Mānoa, and the National Natural Science Foundation of China under Grant 41875055 to the Sun Yat-Sen University. We thank May Izumi for editing the text.

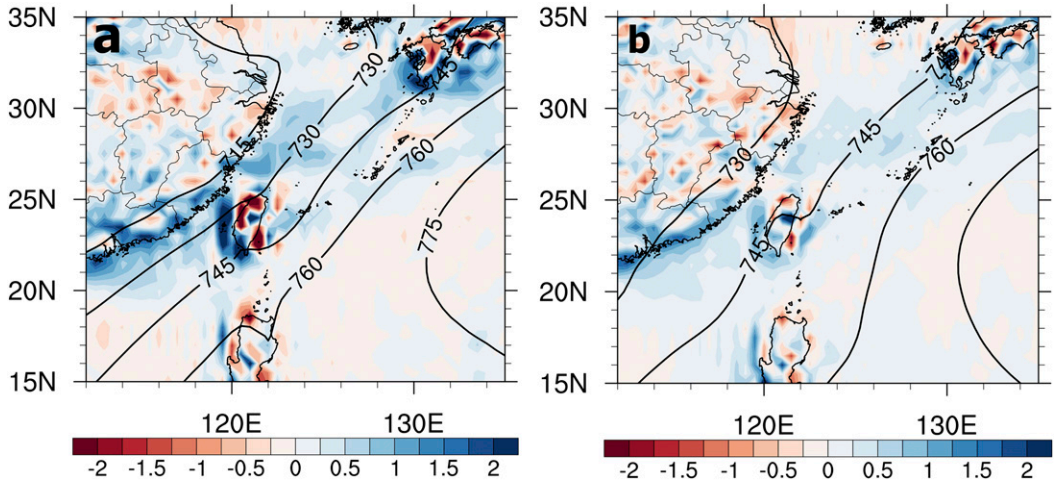

FIG. A1. The 2008–12 CFSR composite horizontal map at the 925-hPa level (a) vertical velocity (w; $cm\,s^{-1}$) and geopotential height (gpm; contoured) for the MBLJ days. (b) As in (a), but for June monthly mean.

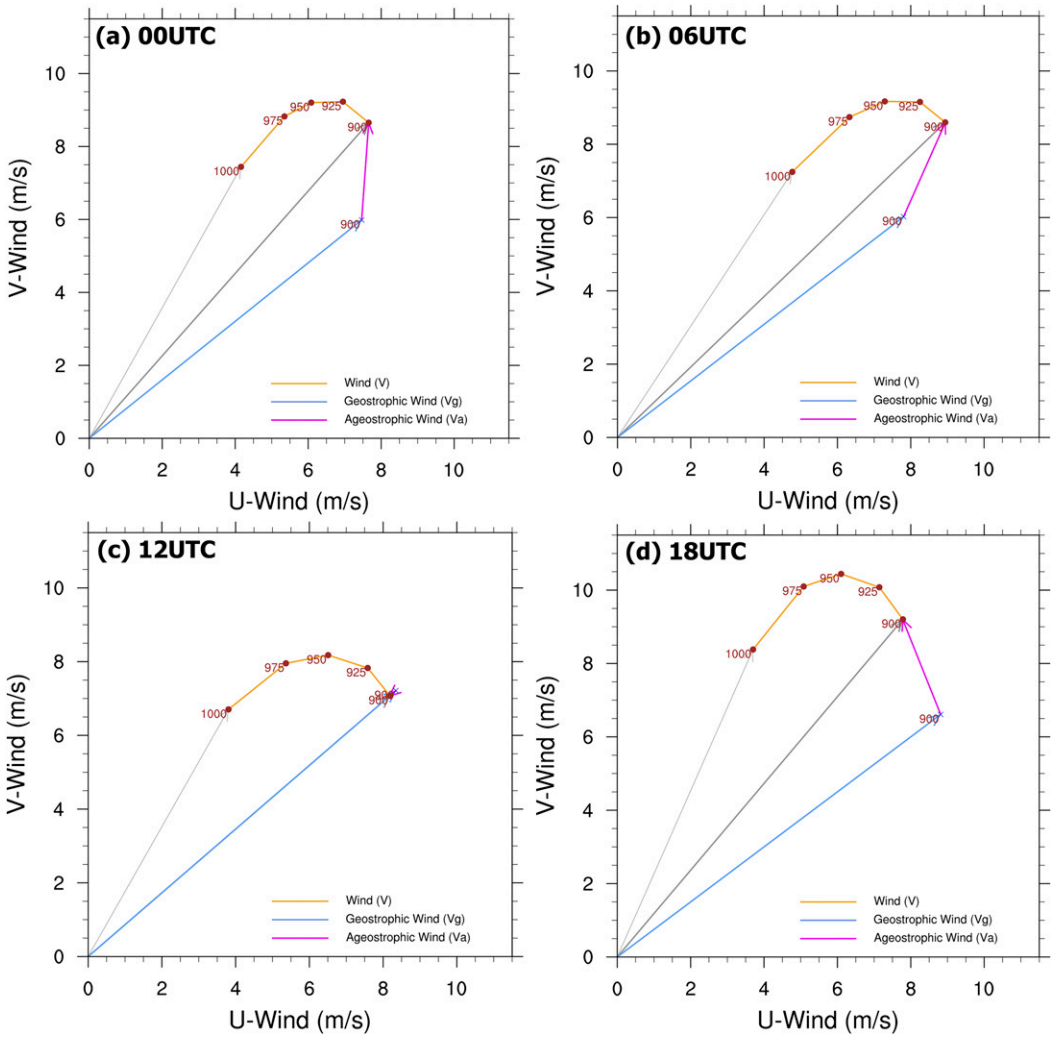

FIG. B1. The hodograph over the boxed area (19°–22°N, 115°–119°E; blue box in Fig. 13) for the MBLJ days; the orange curve is the hodograph from the 1000- to 900-hPa level. The thick black arrow shows the 900-hPa winds (**V**; m s^{-1}). The thick, light blue arrow shows the 900-hPa geopotential winds (Vg; m s^{-1}). The thick, pink arrow shows the 900-hPa ageostrophic wind (Va; m s^{-1}) at (a) 0000 UTC (0800 LST), (b) 0600 UTC (1400 LST), (c), 1200 UTC (2000 LST), and (d) 1800 UTC (0200 LST), respectively.

APPENDIX A

Low-Level Vertical Motion

Figure A1 shows the low-level upward motion associated with the mei-yu trough axis and orographic blocking off the southwestern Taiwan coast when an MBLJ is present, as compared to June monthly mean.

APPENDIX B

Low-Level Wind Profile Throughout the Diurnal Cycle

Figure B1 shows that the wind profile in the MBL resembles an Ekman spiral throughout the diurnal cycle.

REFERENCES

Alpert, J. C., 2004: Sub-grid scale mountain blocking at NCEP. *Proc. 20th Conf. on Weather and Forecasting*, Seattle, WA, Amer. Meteor. Soc., P2.4, http://ams.confex.com/ams/pdfpapers/71011.pdf.

——, M. Kanamitsu, P. M. Caplan, J. G. Sela, G. H. White, and E. Kalnay, 1988: Mountain induced gravity wave drag parameterization in the NMC medium-range forecast model. *Proc. Eighth Conf. on Numerical Weather Prediction*, Baltimore, MD, Amer. Meteor. Soc., 726–733.

——, S.-Y. Hong, and Y.-J. Kim, 1996: Sensitivity of cyclogenesis to lower tropospheric enhancement of gravity wave drag using the Environmental Modeling Center medium-range model. *Proc. 11th Conf. on Numerical Weather Prediction*, Norfolk, VA, Amer. Meteor. Soc., 322–323.

Arya, S. P. S., 1985: The schematics of balance of forces in the planetary boundary layer. *J. Climate Appl. Meteor.*, **24**,

1001–1002, https://doi.org/10.1175/1520-0450(1985)024<1001:TSOBOF>2.0.CO;2.

Blackadar, A. K., 1957: Boundary layer wind maxima and their significance for the growth of nocturnal inversions. *Bull. Amer. Meteor. Soc.*, **38**, 283–290, https://doi.org/10.1175/1520-0477-38.5.283.

Chen, G. T.-J., 1977: An analysis of moisture structure and rainfall for a meiyu regime in Taiwan. *Proc. Natl. Sci. Council*, **1** (11), 1–21.

——, 1978: The structure of a subtropical mei-yu system in Southeast Asia. Taiwan University Department of Atmospheric Sciences Rep. 2, 9–23.

——, and C.-C. Yu, 1988: Study of low-level jet and extremely heavy rainfall over northern Taiwan in the mei-yu season. *Mon. Wea. Rev.*, **116**, 884–891, https://doi.org/10.1175/1520-0493(1988)116<0884:SOLLJA>2.0.CO;2.

Chen, X. A., and Y.-L. Chen, 1995: Development of low-level jets during TAMEX. *Mon. Wea. Rev.*, **123**, 1695–1719, https://doi.org/10.1175/1520-0493(1995)123<1695:DOLLJD>2.0.CO;2.

——, and ——, 2002: Kinetic energy budgets of the low-level jet during TAMEX IOP 5. *J. Meteor. Soc. Japan*, **80**, 1–19, https://doi.org/10.2151/jmsj.80.1.

Chen, Y.-L., and J. Li, 1995a: Characteristics of surface airflow and pressure patterns over the island of Taiwan during TAMEX. *Mon. Wea. Rev.*, **123**, 695–716, https://doi.org/10.1175/1520-0493(1995)123<0695:COSAAP>2.0.CO;2.

——, and ——, 1995b: Large-scale conditions favorable for the development of heavy rainfall during TAMEX IOP 3. *Mon. Wea. Rev.*, **123**, 2978–3002, https://doi.org/10.1175/1520-0493(1995)123<2978:LSCFFT>2.0.CO;2.

——, Y.-X. Zhang, and N. B.-F. Hui, 1989: Analysis of a surface front during the early summer rainy season over Taiwan. *Mon. Wea. Rev.*, **117**, 909–931, https://doi.org/10.1175/1520-0493(1989)117<0909:AOASFD>2.0.CO;2.

——, X. A. Chen, and Y.-Z. Zhang, 1994: A diagnostic study of the low-level jet during TAMEX IOP 5. *Mon. Wea. Rev.*, **122**, 2257–2284, https://doi.org/10.1175/1520-0493(1994)122<2257:ADSOTL>2.0.CO;2.

——, ——, S. Chen, and Y.-H. Kuo, 1997: A numerical study of the low-level jet during TAMEX IOP 5. *Mon. Wea. Rev.*, **125**, 2583–2604, https://doi.org/10.1175/1520-0493(1997)125<2583:ANSOTL>2.0.CO;2.

——, Y.-J. Chu, C.-S. Chen, C.-C. Tu, J.-H. Teng, and P.-L. Lin, 2018: Analysis and simulations of a heavy rainfall event over northern Taiwan during 11–12 June 2012. *Mon. Wea. Rev.*, **146**, 2697–2715, https://doi.org/10.1175/MWR-D-18-0001.1.

Colle, B. A., and D. R. Novak, 2010: The New York Bight jet: Climatology and dynamical evolution. *Mon. Wea. Rev.*, **138**, 2385–2404, https://doi.org/10.1175/2009MWR3231.1.

Cook, K. H., and E. K. Vizy, 2010: Hydrodynamics of the Caribbean low-level jet and its relationship to precipitation. *J. Climate*, **23**, 1477–1494, https://doi.org/10.1175/2009JCLI3210.1.

Dee, D. P., and Coauthors, 2011: The ERA-Interim reanalysis: Configuration and performance of the data assimilation system. *Quart. J. Roy. Meteor. Soc.*, **137**, 553–597, https://doi.org/10.1002/qj.828.

Du, Y., and R. Rotunno, 2014: A simple analytical model of the nocturnal low-level jet over the Great Plains of the United States. *J. Atmos. Sci.*, **71**, 3674–3683, https://doi.org/10.1175/JAS-D-14-0060.1.

——, Q. H. Zhang, Y. Ying, and Y. M. Yang, 2012: Characteristics of low-level jets in Shanghai during the 2008–2009 warm seasons as inferred from wind profiler radar data. *J. Meteor. Soc. Japan*, **90**, 891–903, https://doi.org/10.2151/jmsj.2012-603.

——, ——, Y.-L. Chen, Y. Zhao, and X. Wang, 2014: Numerical simulations of spatial distributions and diurnal variations of low-level jets in China during early summer. *J. Climate*, **27**, 5747–5767, https://doi.org/10.1175/JCLI-D-13-00571.1.

——, Y.-L. Chen, and Q. H. Zhang, 2015: Numerical simulations of the boundary layer jet off the southeastern coast of China. *Mon. Wea. Rev.*, **143**, 1212–1231, https://doi.org/10.1175/MWR-D-14-00348.1.

Garreaud, R., and R. C. Muñoz, 2005: The low-level jet off the west coast of subtropical South America: Structure and variability. *Mon. Wea. Rev.*, **133**, 2246–2261, https://doi.org/10.1175/MWR2972.1.

Holton, J. R., 1967: The diurnal boundary layer wind oscillation above sloping terrain. *Tellus*, **19A**, 199–205, https://doi.org/10.1111/j.2153-3490.1967.tb01473.x.

——, 2004: *An Introduction to Dynamic Meteorology*. 4th ed. Academic Press, 535 pp.

Hong, S.-Y., and H.-L. Pan, 1998: Convective trigger function for a mass-flux cumulus parameterization scheme. *Mon. Wea. Rev.*, **126**, 2599–2620, https://doi.org/10.1175/1520-0493(1998)126<2599:CTFFAM>2.0.CO;2.

Hsiao, F., and Y.-L. Chen, 2014: Revisiting the structure and characteristics of an early summer monsoon trough over South China in 1975. *SOLA*, **10**, 194–198, https://doi.org/10.2151/sola.2014-041.

Huang, W. R., J. C. Chan, and S. Y. Wang, 2010: A planetary-scale land–sea breeze circulation in East Asia and the western North Pacific. *Quart. J. Roy. Meteor. Soc.*, **136**, 1543–1553, https://doi.org/10.1002/qj.663.

Kerns, B., Y.-L. Chen, and M.-Y. Chang, 2010: The diurnal cycle of winds, rain, and clouds over Taiwan during the mei-yu, summer, and autumn rainfall regimes. *Mon. Wea. Rev.*, **138**, 497–516, https://doi.org/10.1175/2009MWR3031.1.

Kim, Y.-J., and A. Arakawa, 1995: Improvement of orographic gravity wave parameterization using a mesoscale gravity wave model. *J. Atmos. Sci.*, **52**, 1875–1902, https://doi.org/10.1175/1520-0469(1995)052<1875:IOOGWP>2.0.CO;2.

Lavers, D. A., G. Villarini, R. P. Allan, E. F. Wood, and A. J. Wade, 2012: The detection of atmospheric rivers in atmospheric reanalyses and their links to British winter floods and the large-scale climatic circulation. *J. Geophys. Res.*, **117**, D20106, https://doi.org/10.1029/2012JD018027.

Li, J., and Y.-L. Chen, 1998: Barrier jets during TAMEX. *Mon. Wea. Rev.*, **126**, 959–971, https://doi.org/10.1175/1520-0493(1998)126<0959:BJDT>2.0.CO;2.

——, ——, and W.-C. Lee, 1997: Analysis of a heavy rainfall event during TAMEX. *Mon. Wea. Rev.*, **125**, 1060–1082, https://doi.org/10.1175/1520-0493(1997)125<1060:AOAHRE>2.0.CO;2.

Lin, Y.-L., 2005: Dynamics of orographic precipitation. *McGraw-Hill 2005 Yearbook of Science & Technology*, McGraw Hill, 248–250.

——, S. Chiao, T.-A. Wang, M. L. Kaplan, and R. P. Weglarz, 2001: Some common ingredients for heavy orographic rainfall. *Wea. Forecasting*, **16**, 633–660, https://doi.org/10.1175/1520-0434(2001)016<0633:SCIFHO>2.0.CO;2.

Liu, Z., D. Ostrenga, W. Teng, and S. Kempler, 2012: Tropical Rainfall Measuring Mission (TRMM) precipitation data and services for research and applications. *Bull. Amer. Meteor. Soc.*, **93**, 1317–1325, https://doi.org/10.1175/BAMS-D-11-00152.1.

Lott, F., and M. J. Miller, 1997: A new subgrid-scale orographic drag parameterization: Its formulation and testing. *Quart. J. Roy. Meteor. Soc.*, **123**, 101–127, https://doi.org/10.1002/qj.49712353704.

Mellor, G. L., 1996: *Introduction to Physical Oceanography*. American Institute of Physics, 284 pp.

Moorthi, S., H. L. Pan, and P. Caplan, 2001: Changes to the 2001 NCEP operational MRF/AVN global analysis/forecast system. NWS Tech. Procedures Bull. 484, 14 pp.

Muñoz, E., A. J. Busalacchi, S. Nigam, and A. Ruiz-Barradas, 2008: Winter and summer structure of the Caribbean low-level jet. *J. Climate*, **21**, 1260–1276, https://doi.org/10.1175/2007JCLI1855.1.

Muñoz, R. C., and R. Garreaud, 2005: Dynamics of the low-level jet off the west coast of subtropical South America. *Mon. Wea. Rev.*, **133**, 3661–3677, https://doi.org/10.1175/MWR3074.1.

Pan, H. L., and W.-S. Wu, 1995: Implementing a mass flux convection parameterization package for the NMC medium-range forecast model. NMC Office Note 409, 43 pp., http://www.ncep.noaa.gov/officenotes/NOAA-NPM-NCEPON-0005/01408A42.pdf.

Parish, T. R., and L. D. Oolman, 2010: On the role of sloping terrain in the forcing of the Great Plains low-level jet. *J. Atmos. Sci.*, **67**, 2690–2699, https://doi.org/10.1175/2010JAS3368.1.

Pham, N. T., K. Nakamura, F. A. Furuzawa, and S. Satoh, 2008: Characteristics of low level jets over Okinawa in the baiu and post-baiu seasons revealed by wind profiler observations. *J. Meteor. Soc. Japan*, **86**, 699–717, https://doi.org/10.2151/jmsj.86.699.

Riehl, H., and J. S. Malkus, 1958: On the heat balance in the equatorial trough zone. *Geophysica*, **6**, 503–537.

Saha, S., and Coauthors, 2010: The NCEP Climate Forecast System Reanalysis. *Bull. Amer. Meteor. Soc.*, **91**, 1015–1058, https://doi.org/10.1175/2010BAMS3001.1.

Sundqvist, H., E. Berge, and J. E. Kristjánsson, 1989: Condensation and cloud parameterization studies with a mesoscale numerical weather prediction model. *Mon. Wea. Rev.*, **117**, 1641–1657, https://doi.org/10.1175/1520-0493(1989)117<1641:CACPSW>2.0.CO;2.

Tao, S. Y., and L. X. Chen, 1987: A review of recent research on the East Asian summer monsoon in China. *Monsoon Meteorology*, C. P. Chang, Ed., Oxford University Press, 60–92.

Trier, S. B., D. B. Parsons, and T. J. Matejka, 1990: Observations of a subtropical cold front in a region of complex terrain. *Mon. Wea. Rev.*, **118**, 2449–2470, https://doi.org/10.1175/1520-0493(1990)118<2449:OOASCF>2.0.CO;2.

Tu, C.-C., Y.-L. Chen, C.-S. Chen, P.-L. Lin, and P.-H. Lin, 2014: A comparison of two heavy rainfall events during the Terrain-Influenced Monsoon Rainfall Experiment (TiMREX) 2008. *Mon. Wea. Rev.*, **142**, 2436–2463, https://doi.org/10.1175/MWR-D-13-00293.1.

——, ——, S.-Y. Chen, Y.-H. Kuo, and P.-L. Lin, 2017: Impacts of including rain-evaporative cooling in the initial conditions on the prediction of a coastal heavy rainfall event during TiMREX. *Mon. Wea. Rev.*, **145**, 253–277, https://doi.org/10.1175/MWR-D-16-0224.1.

Witcraft, N. C., Y.-L. Lin, and Y.-H. Kuo, 2005: Dynamics of orographic rain associated with the passage of a tropical cyclone over a mesoscale mountain. *Terr. Atmos. Ocean*, **16**, 1133–1161, https://doi.org/10.3319/TAO.2005.16.5.1133(A).

Xu, W., E. J. Zipser, Y.-L. Chen, C. Liu. Y.-C. Liou, W.-C. Lee, and B. Jou, 2012: An orography-associated extreme rainfall event during TiMREX: Initiation, storm evolution, and maintenance. *Mon. Wea. Rev.*, **140**, 2555–2574, https://doi.org/10.1175/MWR-D-11-00208.1.

Yanai, M., S. Esbensen, and J.-H. Chu, 1973: Determination of bulk properties of tropical cloud clusters from large-scale heat and moisture budgets. *J. Atmos. Sci.*, **30**, 611–627, https://doi.org/10.1175/1520-0469(1973)030<0611:DOBPOT>2.0.CO;2.

Yeh, H.-C., and Y.-L. Chen, 2002: The role of offshore convergence on coastal rainfall during TAMEX IOP 3. *Mon. Wea. Rev.*, **130**, 2709–2730, https://doi.org/10.1175/1520-0493(2002)130<2709:TROOCO>2.0.CO;2.

——, and ——, 2003: Numerical simulations of the barrier jet over northwestern Taiwan during the mei-yu season. *Mon. Wea. Rev.*, **131**, 1396–1407, https://doi.org/10.1175/1520-0493(2003)131<1396:NSOTBJ>2.0.CO;2.

Zhang, D.-L., S. Zhang, and S. J. Weaver, 2006: Low-level jets over the Mid-Atlantic states: Warm-season climatology and a case study. *J. Appl. Meteor. Climatol.*, **45**, 194–209, https://doi.org/10.1175/JAM2313.1.

Zhao, Q. Y., and F. H. Carr, 1997: A prognostic cloud scheme for operational NWP models. *Mon. Wea. Rev.*, **125**, 1931–1953, https://doi.org/10.1175/1520-0493(1997)125<1931:APCSFO>2.0.CO;2.

Zhu, Y., and R. E. Newell, 1998: A proposed algorithm for moisture fluxes from atmospheric rivers. *Mon. Wea. Rev.*, **126**, 725–735, https://doi.org/10.1175/1520-0493(1998)126<0725:APAFMF>2.0.CO;2.